Published in final edited form as:
J Immunol. 2013 October 1; 191(7): 3764–3777. doi:10.4049/jimmunol.1202556.

Inhibition of endogenous activated protein C attenuates experimental autoimmune encephalomyelitis by inducing myeloid-derived suppressor cells[1]

Leah M. Alabanza[*], **Naomi L. Esmon**[#], **Charles T. Esmon**[†], and **Margaret S. Bynoe**[*,2]

[*]Department of Microbiology and Immunology, College of Veterinary Medicine, Cornell University, Ithaca, NY 14853

[#]Coagulation Biology Laboratory, Oklahoma Medical Research Foundation, and Department of Pathology, University of Oklahoma Health Sciences Center, Oklahoma City, OK 73104

[†]Coagulation Biology Laboratory, Oklahoma Medical Research Foundation, Howard Hughes Medical Institute, and Departments of Pathology and Biochemistry and Molecular Biology, University of Oklahoma Health Sciences Center, Oklahoma City, OK 73104

Abstract

Activated protein C (APC) is an anti-coagulant involved in the interactions between the coagulation and immune systems. APC has broad anti-inflammatory effects mediated through its ability to modulate leukocyte function and confer vascular barrier protection. We investigated the influence of APC on the pathogenesis of experimental autoimmune encephalomyelitis (EAE), the animal model for multiple sclerosis. We modulated APC levels in the circulation during EAE induction through systemic administration of a monoclonal antibody against protein C/APC (anti-PC). We initially hypothesized that inhibition of APC may result in a heightened inflammatory environment leading to increased EAE pathogenesis. Contrary to this hypothesis, mice treated with anti-PC antibody exhibited attenuated EAE. Interestingly, despite reduced disease severity and minimal pathogenic conditions in the CNS, anti-PC mice exhibited considerable leukocyte infiltration in the brain, comparable to control mice with severe EAE. Furthermore, $CD4^+$ T-cells were diminished in the periphery of anti-PC mice while various $CD11b^+$ populations were increased, notably the myeloid-derived suppressor cells (MDSC), a $CD11b^+$ subset characterized as potent T-cell suppressors. MDSCs from anti-PC mice exhibited increased expression of T-cell-suppressive factors and effectively inhibited T-cell proliferation. Overall, our findings show that APC inhibition affected EAE pathogenesis at multiple fronts; specifically, increasing vascular barrier permeability, as evidenced by considerable leukocyte infiltration in the brain. APC inhibition, additionally, modulated the functional responses of $CD11b^+$ cells leading to the expansion and increased activation of MDSCs, which are suppressive to the $CD4^+$ T-cells required for EAE progression, thereby resulting in attenuated EAE.

Introduction

The anti-coagulant, APC, has a prominent role in mediating the complex crosstalk between the coagulation and inflammatory responses (1–3). APC is a serine protease derived from

[1]This work was funded by NIH Grant R01 NS063011 (to M.S.B.)

[2] Corresponding author: Margaret S Bynoe, msb76@cornell.edu, Phone: 607-253-4023, Fax: 607-253-338.

Disclosures:
The authors declare no competing financial interest.

the zymogen protein C (PC), which is activated on the surface of endothelial cells by the coagulation factor, thrombin bound to the glycoprotein, thrombomodulin (3). Once activated, APC in the circulation is known for regulating blood clotting through its ability to proteolytically inactivate coagulation factors Va and VIIIa, consequently dampening further generation of thrombin (4). Independent of APC's function in the coagulation cascade, APC can affect various cellular processes through its interactions with membrane receptors. APC mediates cell signaling in endothelial cells through binding with endothelial protein C receptor (EPCR), enabling APC to activate the G-protein coupled receptor, protease-activated receptor-1 (PAR-1) (5, 6). APC-mediated activation of PAR-1 on endothelial cells reduces endothelial permeability through stabilization of cytoskeletal components (7), consequently limiting the extravasation of inflammatory leukocytes (5). APC additionally directs leukocyte function through alteration of signaling pathways involved in inflammatory responses (8–12). Several studies have proposed that APC's effects on leukocytes may similarly be mediated through the EPCR/PAR-1 pathway (13, 14). However, a more recent study has shown that APC's anti-inflammatory effects on myeloid cells are mediated through the binding of APC to the CD11b integrin (15).

The pleiotropic effects of APC, which encompasses both cell signaling and anticoagulant properties, are indicative of its broad influence in various disease conditions and its potential as a promising therapeutic target. The efficacy of APC as a therapeutic molecule has, in fact, already been demonstrated for severe sepsis. In the PROWESS study, infusion of human recombinant APC improved survival among patients with severe sepsis (16). The effectiveness of APC in sepsis treatment however remains controversial since its efficacy was not exhibited in a subsequent trial (17), prompting the withdrawal of the drug from the market (18). Nevertheless, APC's protective effects in other disease settings have been evidenced in various animal studies. In ischemic stroke models, APC can reduce leukocyte infiltration in the brain (19), and APC can ameliorate the animal model for amyotrophic lateral sclerosis (ALS) by conferring blood-spinal cord barrier protection (20). APC has also been demonstrated to attenuate inflammation in mouse models for inflammatory bowel disease (IBD) (21) and lung injury model (22).

In this study, we set out to investigate the influence of endogenous APC on the pathogenesis of EAE, the animal model for multiple sclerosis (MS). EAE and MS are autoimmune disorders characterized by neuroinflammation and consequent axonal demyelination leading to clinical symptoms such as paralysis (23, 24). The neuroinflammatory response in EAE is mainly mediated by effector $CD4^+$ T-cells that are able to infiltrate the central nervous system (CNS) as a result of permeability and dysfunction at CNS barriers (25). Our rationale for studying APC in EAE stems from previous studies suggesting the likely involvement of endogenous coagulation components in EAE and MS pathology. In a study by Han et. al, proteomics analysis of MS lesions revealed the presence of coagulation proteins in chronic active plaques (26). In EAE studies, fibrin deposition in the brain has been reported (27), and increased presence of thrombin inhibitors were detected in the peripheral circulation of EAE mice (28). Moreover, APC's known anti-inflammatory effects, specifically its ability to mediate leukocyte function and confer vascular barrier protection, further underscore the relevance of studying APC in EAE, wherein the major pathological component is CNS barrier dysfunction resulting in neuroinflammation and pathology.

To investigate APC function in EAE, we inhibited endogenous APC during disease progression through systemic administration of an antibody against protein C/APC (anti-PC). We anticipated that blocking APC may lead to worsening of EAE due to CNS barrier dysfunction and/or by exacerbating systemic inflammation. Contrary to our hypothesis, we observed that mice treated with anti-PC exhibited attenuated clinical signs despite considerable leukocyte infiltration in the brain. Moreover, we observed diminished T-cell

effector function in these mice, coupled with increased expansion of MDSCs, a cell-subset characterized as potent T-cell supressors (29). This study shows that diminished APC activity can affect EAE pathogenesis at multiple fronts, influencing both BBB permeability and effector functions of leukocytes. The results of this study exemplify the intricate and multi-faceted interaction between the coagulation and immune systems, which is further complicated by each unique disease setting.

Materials and Methods

Mice and EAE induction

C57BL/6 (BL/6) mice and C57BL/6 2d2 TCR transgenic mice were generated from our in-house breeding colony or were purchased from Taconic (Germantown). Mice were maintained in specific pathogen-free facility at Cornell University. Procedures performed on mice were approved by the Institutional Animal Care and Use Committee of Cornell University. To induce EAE, a 1:1 emulsion of myelin oligodendrocyte glycoprotein peptide ($MOG_{35–55}$) (Anaspec) at 1 mg/ml and complete Freund's adjuvant (CFA) (Sigma) was subcutaneously injected into mice flanks. Pertussis toxin (PTX) (List Biologicals) at 20 ng/ml was intravenously injected on the day of immunization, and a second dose was administered 48 hours later. Clinical scores were assigned as follows: 0 = no disease, 0.5 = weak tail, 1 = completely limp tail, 1.5 = impaired righting reflex, 2 = affected gait, 2.5 = partial hind limb paralysis, 3 = complete hind limb paralysis, 3.5 = hind limb and partial forelimb paralysis, 4 = moribund, 5 = death. Mice that reach a score of 4 are euthanized and scored as 5.

Antibody to protein C

Generation of mAb MPC1609 (anti-PC) was described previously (30). Anti-PC was raised to mouse PC and cross reacts with mouse APC. Anti-PC inhibits the activation of protein C and blocks both PC and APC from binding to endothelium and phospholipid surfaces, thus effectively abrogating APC's anticoagulant and cell signaling capabilities (30). The antibody at 1mg/kg was administered via intraperitoneal (i.p) injection.

Immunohistochemistry

CNS harvested after perfusion were snap frozen in OCT media (Tissue-Tek, CA). Frozen tissues were sectioned to 6-micron thickness using a cryostat, and sections were affixed to Superfrost Plus slides (Fisher). After fixing in acetone, slides were washed in PBS and blocked with casein (Vector Labs) for 10 minutes. Slides were incubated with primary antibodies for 90 minutes at 37°C. Primary antibodies used are as follows: anti-CD45 (AbD Serotec) anti-Iba-1 (Wako Chemicals), anti-MOG (R&D Systems). After washing, slides were incubated with the appropriate secondary antibody for 30 minutes, washed and subsequently incubated with avidin-horseradish peroxidase (HRP) complex (Invitrogen). Slides were developed with chromogenic substrate for HRP (Zymed) and counterstained with hematoxylin. Images were captured using a Zeiss Axio Imager M1 microscope.

CNS Infiltrate and Splenocyte Isolation

CNS harvested after perfusion were homogenized using a syringe plunger. Tissues were further homogenized by repeatedly passing through a syringe with an 18-gauge blunt needle. CNS homogenates were fractionated on 30/70% Percoll gradient, and cells were recovered from the 30/70 interface. For splenocyte isolation, spleens were homogenized between the frosted ends of two glass slides. Homogenates were re-suspended in ACK lysis buffer to lyse erythrocytes. After washing, splenocytes were passed through a 7μm cell strainer and prepared for flow cytometry analysis or cutured *in vitro*.

Flow Cytometry

Cells were re-suspended in staining buffer (PBS with 0.5% BSA, and 0.09% sodium azide). Cell suspensions were incubated with Fc block (BD Biosciences) for 10 minutes before incubation with primary antibodies for 30 minutes at 4°C. Primary antibodies used are as follows: PE-conjugated anti-mouse CD4 (BD Biosciences), CD11b (eBioscience), CTLA-4 (BD Biosciences), FITC-conjugated anti-mouse CD8 (BD Biosciences), CD69, PerCP-conjugated anti-mouse CD25, NK1.1 (eBioscience), B220 (BD Biosciences), allophycocyanin-conjugated anti-mouse Ly6C, CD11c (eBioscience). Foxp3 staining was done with the Ebioscience Foxp3 staining kit in accordance with the manufacture's protocol. For iNOS intracellular staining, cells were fixed in 4% paraformaldehyde and permeabilized with .01% triton-x. Cells were incubated with polyclonal rabbit anti-mouse iNOS (BD Biosciences) for 30 minutes. Cells were washed and subsequently incubated with allophycocyanin-conjugated secondary antibody. For annexin V staining, we used the BD Pharmingen Apoptosis Detection Kit and followed the manufacturer's protocol. All samples were acquired using a FACSCanto II flow cytometer (BD Biosciences). Raw data were evaluated using FlowJo Flow Cytometry Analysis Software (Treestar).

Dextran Extravasation Assay

At day 5 post EAE induction, 2 mg of texas red-labeled dextran (10,000 molecular weight) were i.v. injected into the systemic circulation. 5 hours after dextran injection, mice were perfused, and brains were harvested. Brains were homogenized in 50 mM Tris-HCl (1:1 per μl Tris-HCl to mg of brain weight). Homogenates were centrifuged and supernatants were collected. Supernatants were mixed 1:1 with methanol and centrifuged. Fluorescence in supernatants was quantified using a BioTeck (Winnoski, VT) Synergy 4 plate reader. Dextran concentration was based on a standard curve.

In vitro cell culture and ELISA

Cells were cultured in complete RPMI (10% FBS, Penicillin/Streptomycin, L-glutamine, Sodium Pyruvate, 50mM 2-Mercaptoethanol, 25mM HEPES buffer). Samples were cultured untreated or stimulated with $MOG_{35–55}$ (10 μg/ml) for 48 hours. After culture, supernatants were collected for ELISA. ELISA for IFN-γ and IL-10 (eBioscience) were performed according to the manufacturer's protocol.

Proliferation Assay

Splenocytes were labeled with CFSE (Molecular Probes, NY) according to the manufacturer's protocol. T-cells in whole-splenocyte culture were stimulated with plate-bound anti-CD3 (1μg/ml) (Ebioscience) and soluble anti-CD28 (1μg/ml) (Biolegend) for 96 hours. After culture, splenocytes were labeled with PE-conjugated mouse anti-CD4 and acquired by flow cytometry to assess CFSE dilution. For $CD11b^+/CD4^+$-cell co-culture, splenic $CD11b^+$ cells were isolated using Easy Sep positive selection kit (Stem Cell Technologies), and splenic MOG-specific $CD4^+$ T-cells from naive BL/6 2D2 transgenic mice were isolated using Easy Sep $CD4^+$ selection kit (Stem Cell Technologies). Cell isolation was done according the manufacturer's protocol. $CD4^+$ T-cells were labeled with CFSE, stimulated with $MOG_{35–55}$ (10 μg/ml) and co-cultured with $CD11b^+$ cells for 96 hours at a ratio of 1:4. Proliferation was assessed by flow cytometry based on CFSE dilution.

Quantitative real-time PCR

Mice were perfused, and CNS were harvested and homogenized. Total RNA was extracted using Trizol (Invitrogen) according to the manufacturer's protocol. Extracted RNA was treated with Baseline-Zero DNAse (Epicentre) to remove contaminating genomic DNA. 1.5

μg of total RNA was reverse transcribed using High-Capacity cDNA Reverse Transcription kit (Applied Biosystems). Real Time PCR was performed using SYBR Green technology (SYBR FAST Master Mix KAPAbiosystems) on a CFX96 Real Time System Thermal Cycler (Bio-RAD). The cycling conditions were as follows: Enzyme activation 95° C for 3 minutes followed by 40 cycles of denaturation 95°C for 3 secs, annealing 60° C for 30 seconds, elongation 72° C for 5 seconds. BioRad CFX Manager software was used to determine cycle threshold (C_t) values, and gene expression levels were calculated using the $2^{-\Delta\Delta Ct}$ method. Gene expression levels were normalized to the internal control gene, GAPDH.

Arginase Activity

Splenocytes were lysed with lysis buffer (0.1% triton-X, pepstatin 5μg, aprotinin 5μg, and antipain 5μg). Arginase activity was measured as described previously (31). Sample absorbance was read with a Biotek EL x 50 plate reader at 550 nm.

Griess Assay

Splenocytes were cultured and supernatants were collected after 48 hours. Assay was done as described previously (32). Absorbance was measured in a Biotek EL x 50 plate reader at 550 nm.

Reactive Oxygen Species

Splenocytes were labeled with anti-Ly6C and anti-CD11b. Cells were washed and incubated with 10 uM of 2′,7′-Dichlorofluorescein diacetate (Sigma) for 30 minutes at 37°C. Cells were washed and acquired by flow cytometry to assess ROS generation.

Immunofluorescence

Splenocytes were cultured on coverslips in 24-well plates. After culture, cells were washed and stained with FITC-conjugated anti-mouse CD11b (eBioscience) and allophycocyanin-conjugated anti-Ly6C (Ebioscience). Cells were fixed with 4% PFA and permeabilized with 0.1% triton-X. Cells were stained with polyclonal anti-arginase I (Genetex) and subsequently incubated with the appropriate secondary antibody. After washing, coverslips were treated with Prolong Gold with Dapi (Molecular Probes) and mounted on slides. Images were captured using a Zeiss Axio Imager M1 microscope.

Statistical Analyses

Statistical analyses were performed using GraphPad Prism 5 software. Statistical significance was assessed by unpaired Student *t* test or by Mann Whitney Test as indicated in figure legends.

Results

Inhibition of endogenous APC attenuates EAE

To determine whether APC can influence EAE pathogenesis, we inhibited endogenous APC in the circulation through administration of a monoclonal antibody to PC/APC (See Materials and Methods). Anti-PC or IgG isotype at 10 mg/kg was administered at days 0, 2, 4, and 6 post EAE induction. Administration of anti-PC within this timeframe inhibits APC during the initiation phase of the immune response, as well as at the outset of the effector phase of EAE, which is characterized by leukocyte infiltration into the CNS. We observed that the onset of clinical signs in mice treated with anti-PC (anti-PC mice) was significantly delayed (Fig. 1A–B). The mean day of onset for anti-PC mice was 16.7 days post EAE induction while the controls exhibited clinical symptoms as early as day 7 with mean onset

at 10.5 days post immunization. Additionally, incidence of disease was higher in the control group; 80% of controls developed EAE by day 16 and 100% exhibited paralysis by day 22 (Fig. 1C). In contrast, only 44% of anti-PC mice exhibited clinical signs on day 16 and 66% by day 22. These data show that inhibition of endogenous APC can alter the disease course of EAE, albeit in a rather unexpected way, given that inhibition of APC, an anti-inflammatory molecule, attenuated EAE rather than increasing disease severity.

The major pathological component in EAE is leukocyte infiltration into the CNS, which typically correlates with the severity of clinical signs (24, 25). To investigate why anti-PC mice had attenuated EAE, we assessed the severity of CNS infiltration at the peak of disease (days 14–17). The extent of leukocyte ($CD45^+$ cells) infiltration in the brains of control mice positively correlates with disease severity (Fig. 1E). Interestingly, 33% of anti-PC mice (Sup. Table I) with no clinical signs had considerable $CD45^+$ infiltrates in the brain, comparable to controls with severe EAE (Fig. 1E–F). We noted that cellular infiltrates were located in similar areas of the brain in both groups, notably in the brain parenchyma adjacent to the lateral ventricles (Fig.1E upper panel), in the cerebellar parenchyma (Fig. 1E lower panel), and at the meninges (data not shown). We additionally observed that the extent of infiltration in the spinal cords (SC) of controls corresponds with the severity of paralysis (Fig. 1G). Interestingly, the degree of cellular infiltration in the SC of anti-PC mice was minimal despite considerable infiltration in the brain (Figure 1G–H). Perivascular cuffing, characterized by cellular infiltrates encircling blood vessels in the CNS, is a hallmark of EAE pathology and is indicative of BBB permeability (33). We observed perivascular cuffing in the brain parenchyma of anti-PC mice (Fig. 1I), an indication of BBB permeability in these mice. To assess any alterations in the degree of BBB permeability between the two groups, fluorescent dextran molecules were injected into the systemic circulation of both IgG and anti-PC mice, and we examined the degree of dextran extravasation into the brain. We consistently observed increased dextran extravasation in the brains of anti-PC mice compared to controls and naïve mice (Fig. 1J), indicating increased BBB permeability in anti-PC mice. Overall, these data show that despite showing attenuated clinical signs, anti-PC mice exhibit increased BBB permeability as evidenced by pronounced leukocyte infiltration in the brain as well as increased dextran extravasation in the brain.

Anti-PC mice exhibit reduced pathogenic and inflammatory conditions in the CNS

To further investigate the disparity in disease course between anti-PC and control mice, we next examined the composition of cellular infiltrates in the CNS. We did not observe significant differences in $CD4^+$ T-cell frequency and absolute numbers in the brains (Fig. 2A–B) and SC (Fig. 2E) between the two groups. Various $CD4^+$ T-cell subsets have differing effects on EAE severity; specifically, the T-regulatory (T-reg) subset ($CD4^+CD25^+Foxp3^+$) confers protection in EAE, while T-helper 1 (Th1) and T-helper 17 (Th17) subsets are pathogenic (25). We observed significantly increased T-reg frequency in the brains of anti-PC mice compared to controls (Fig. 2C–D). T-reg frequency is similarly increased in the SC of anti-PC group, although the difference did not reach statistical significance (Fig. 2F). The protective effect of T-regs is partly mediated through the production of the anti-inflammatory cytokine, IL-10 (34). Consistent with increased T-reg frequency, we detected increased IL-10 production from cellular infiltrates in the brains and SC of anti-PC mice (Fig. 2G). In contrast, the production of the Th1 cytokine, IFN-γ, is reduced from brain infiltrates (but not from SC infiltrates) in anti-PC mice (Fig. 2H). We similarly detected decreased IL-17 mRNA expression in the brains and SC of anti-PC compared to controls (Fig. 2I), suggesting reduced pathogenic T_H17 subset in the CNS of anti-PC mice. Collectively, these data show that despite considerable infiltration in the brains of anti-PC mice, the pathogenic $CD4^+$ subsets and their respective signature cytokines

required for disease progression are reduced while the suppressive T-reg population is increased. We additionally examined the frequency and absolute numbers of other leukocytes populations in the brain but found no considerable differences (Sup. Fig.1).

We next examined the extent of CNS pathology in control and anti-PC mice. Activated microglial cells greatly contribute to CNS pathology in EAE, including demyelination, axonal pathology and neurodegeneration, leading to the clinical signs of the disease (35, 36). Control mice with severe EAE showed markedly pronounced staining for the microglial marker, Iba-1, (Fig. 2J), suggesting increased microglial activation (35, 36) in these mice. In contrast, the brains of anti-PC mice show reduced Iba-1 staining (Fig. 2J), indicative of minimal microglial activation in these mice. We additionally assessed the extent of demyelination in the CNS of both groups and detected extensive demyelination in the brains and SC of control mice, correlating with the severity of clinical signs (Fig. 2K). Conversely, the CNS of anti-PC mice showed minimal demyelination (Fig. 2K). Taken together, the reduced microglial activation and demyelination further demonstrate the decreased inflammatory and pathogenic conditions in the CNS of anti-PC mice despite the presence of cellular infiltrates.

Peripheral CD4$^+$ T-cells in anti-PC mice are significantly reduced

In EAE, leukocyte infiltration in the CNS is preceded by initial activation of the immune response in the periphery (37). Since APC is known to directly modulate various leukocyte functions (9, 13), we hypothesize that abrogating APC in the circulation at the initiation of EAE can likely affect the activation and functional responses of peripheral leukocytes. We, therefore, examined the frequency and functional characteristics of various leukocyte populations in the periphery. We observed significantly decreased splenic CD4$^+$ T-cells in anti-PC mice compared to controls (Fig. 3A–B). Consistent with what we observed in the CNS, the frequency of T-regs is also significantly increased in the periphery of anti-PC mice (Fig. 3C–D). We evaluated the expression levels of various cell surface markers on splenic T-cells. Interestingly, we observed that the ratio of CD3^{high} to CD3^{low} T-cells is consistently reduced in anti-PC mice compared to controls (Fig. 3E). The expression levels of other CD4$^+$ T-cell surface markers, however, were not considerably altered (Fig. 3F). We next assessed the proliferative capacity of splenic CD4$^+$ T-cells from both experimental groups. CD4$^+$ T-cells in whole-splenocyte culture were re-stimulated *in vitro*. We observed that CD4$^+$ T-cell from control mice exhibited robust proliferation, while the proliferative capacity of CD4$^+$ T-cells from anti-PC mice is significantly diminished (Fig. 2G). Taken together, these data are indicative of a decreased and deficient CD4$^+$ T-cell effector function in anti-PC mice.

Various CD11b$^+$ populations including myeloid-derived suppressor cells are significantly increased in the periphery of anti-PC mice

While we did not observe significant changes in the frequencies of various non-T-cell populations between the two experimental groups (data not shown), we did observe increased frequencies (Fig. 4A–B) and absolute cell counts (Fig. 4C) of splenic CD11b$^+$ cells in anti-PC mice compared to controls, and this was consistent through different time points in EAE (Fig. 4B). Since various leukocyte subsets are known to express CD11b, we next determined the frequency of specific CD11b-expressing leukocyte subsets. We observed significantly increased dendritic cells (CD11b$^+$CD11c$^+$) (Fig. 4D upper panel) and macrophages (CD11b$^+$F480$^+$) (Fig. 4D lower panel) and in anti-PC mice. Another population of cells known to express CD11b are myeloid-derived suppressor cells (MDSC), which are a subset of cells notably characterized to be potent T-cell suppressors (29, 38, 39). Various studies have used the co-expression of CD11b and Ly6C as identifying markers for MDSC in mice (29, 40). Consistent with other CD11b $^+$ populations, we observed increased

frequency (Fig. 4E–F) and absolute cell numbers (Fig. 4G) of MDSCs in anti-PC mice, and this was observed through various stages in EAE (Fig. 4F). MDSCs are divided into a monocytic ($CD11b^+Ly6C^{high}Ly6G^-$) and granulocytic ($CD11b^+Ly6C^{low}Ly6G^+$) subsets (29). We observed significantly increased numbers of both subsets in anti-PC mice (Fig. 4H). MDSCs from anti-PC mice also exhibit significantly increased IL-4 receptor α (IL-4Rα) (Fig. 4I), a characteristic cell surface marker on some MDSC subpopulations and has been implicated in their suppressive functions (39). We also examined the expression of other surface markers on MDSCs, specifically PDL-1, CD40, MHCII, and B7.1, but found no significant differences between control and anti-PC cells (Fig 4I).

$CD11b^+$ cells from anti-PC mice exhibit high levels of Arginase I activity, iNOS expression, and increased reactive oxygen species production

Several studies have demonstrated that the suppressive effects of MDSC on T-cells is largely mediated through arginase I (Arg I) activity, nitric oxide (NO) production, and generation of reactive oxygen species (29, 39). Increased Arg I activity in MDSCs depletes L-Arg from the microenvironment, resulting in suppression of various T-cell responses, including inhibition of T-cell proliferation, reduced CD3ζ chain expression, and in some studies, increased Arg I activity has been implicated in MDSC-mediated T-reg expansion (39–41). We assessed higher arginase activity in splenocytes from anti-PC mice (Fig. 5A), and we additionally show by immunofluorescence staining that Arg I is expressed by $CD11b^+$ and $CD11b^+$ $Ly6C^+$ cells (Fig. 5B). MDSCs are also known to express elevated levels of iNOS, which similarly utilizes L-Arg as a substrate to produce nitric oxide (NO), thus contributing to L-Arg depletion (29, 39). We observed significantly increased iNOS expression in $CD11b^+$ and $CD11b^+Ly6C^+$ populations from anti-PC mice (Fig. 5C), coupled with elevated NO production (Fig. 5D). Another mechanism for MDSC-mediated T-cell suppression has been attributed to the generation of ROS, known to inhibit antigen-specific T-cell proliferation and downregulate CD3ζ chain expression (29, 39). We observed significantly increased ROS positive $CD11b^+$ (Fig. 5E) and $Ly6C^+$ (Fig. 5G) cells from anti-PC mice, as well as elevated generation of ROS in these cells (Fig. 5F & 5H) Collectively, these data demonstrate that $CD11b^+$ cells from anti-PC mice express and generate elevated levels of factors that have been specifically implicated in T-cell supression.

$CD11b^+$ cells from anti-PC mice suppress $CD4^+$ T-cell proliferation and mediate T-reg expansion

We hypothesize that the diminished $CD4^+$ T-cell numbers (Fig. 3A–B) is a consequence of increased expansion of suppressive $CD11b^+$ cells, notably MDSCs. We tested this hypothesis by isolating $CD11b^+$ cells from both groups and examined their ability to suppress the proliferation of $MOG_{35–55}$-specific $CD4^+$ T-cells. We observed that $CD11b^+$ cells from anti-PC mice were more effective in suppressing $MOG_{35–55}$-induced proliferation of $CD4^+$ T-cells compared to $CD11b^+$ cells from controls (Fig. 6A). No difference in proliferation, however, was observed if $CD4^+$ T-cells were co-cultured with non-$CD11b^+$ cells from either anti-PC or control mice (Fig. 6B). Moreover, we observed that $CD4^+$ T-cells co-cultured with $CD11b^+$ cells from anti-PC mice resulted in significantly lowered percentage of $CD3^{high}$ T-cells (Fig. 6C). A number of studies have shown that MDSCs can directly mediate T-reg expansion. We postulate that the increased frequency of T-regs, which was observed both in the CNS (Fig. 2C–D) and periphery (Fig. 3C–D) of anti-PC mice, is similarly mediated by MDSCs in these mice. We tested this hypothesis by co-culturing *in vitro*-stimulated $CD4^+$ T-cells with $CD11b^+$ cells from either anti-PC or control mice. We observed significantly higher frequency of T-regs (Fig. 6D) and increased CD25 expression on T-regs (Fig. 6E) following co-culture with $CD11b^+$ cells from anti-PC mice. We next assessed the capacity of $CD11b^+$ cells from anti-PC mice and control mice to directly suppress EAE progression by adoptively transferring $CD11b^+$ from either group to

EAE recipient mice. We observed that recipient mice that received Cd11b$^+$ cells from anti-PC mice developed attenuated EAE (Fig. 6F). Altogether, these data demonstrate the suppressive capacity of CD11b$^+$ cells from anti-PC mice in suppressing T-cell function and EAE progression.

APC directly binds to MDSCs

While APC has traditionally been known to regulate leukocyte function through its interaction with the receptor, EPCR, several studies have also demonstrated that APC can regulate the cellular processes of leukocytes by binding with receptors other than EPCR (42, 43). One particular study by Cao et al. has shown that APC directly binds the CD11b integrin on CD11b$^+$ cells, enabling APC to co-localize and activate PAR-1 on the cell surface, subsequently resulting in the down regulation of pro-inflammatory responses in CD11b$^+$ cells (15). Based on this study, we hypothesize that APC can negatively regulate the CD11b$^+$ population, including MDSCs, during the progression of EAE. We confirmed that MDSCs express PAR-1 (Fig. 7A), suggesting that these cells express the necessary receptor to be responsive to APC regulation. We next determined whether APC can directly interact with MDSCs. Fluorochrome-conjugated APC's were incubated with splenocytes, and we show by flow cytometry that APC directly binds the Ly6C$^+$ population (Fig. 7B). Moreover, we confirm that the monoclonal antibody used to inhibit APC in EAE mice can abrogate the direct binding of APC to Ly6C$^+$ cells (Fig. 7C). We also show that blocking the CD11b integrin similarly decreases the binding of APC to Ly6C$^+$ cells (Fig. 7D), confirming that APC binds the CD11b$^+$ integrin on these cells. MDSCs are known to expand under various inflammatory conditions, including during EAE. We postulate that since APC has been shown to be a negative regulator of CD11b$^+$ cells (15), inhibiting APC in the circulation during inflammatory conditions in EAE likely contributed to the increased expansion and activation of CD11b cells, notably the MDSCs. We observed that inhibiting APC in the circulation of naïve mice did not affect the frequency of CD11b$^+$ and MDSC population (Sup. Fig. 2A–B), indicating that APC's effect on CD11b$^+$ and MDSC expansion is mediated under inflammatory conditions. The expansion and increased survival of MDSCs during pathogenic conditions have been attributed to Stat-3 signaling (39, 44). Interestingly, it has been demonstrated previously that APC can decrease the expression of Stat-3 in CD11b$^+$ cells through APC's interaction with the CD11b integrin (15). Consistently, we observed increased Stat-3 expression (Fig. 7E) and activation (Fig. 7F) in CD11b$^+$ cells from anti-PC mice. Stat-3 expression in MDSCs has been known to drive cell survival by upregulating anti-apoptotic genes. Accordingly, we observed decreased apoptosis (Fig. 7G) in MDSCs from anti PC mice, likely contributing to the increase in MDSC numbers in these mice. Collectively these data demonstrate that APC directly interacts with Ly6C$^+$ cells, indicative of the potential regulatory capability of APC on MDSCs, likely by modulating Stat3 expression and thus affecting expansion and cell survival of this leukocyte subset.

Discussion

In addition to its traditional function as an anti-coagulant, APC affects various aspects of the pathological setting by directing cellular processes involved in inflammatory responses, vascular integrity, and cell survival (1–3). Our study further exemplifies the broad-ranging effects of APC in pathological conditions. We observed that depletion of APC during EAE affected disease pathogenesis at multiple fronts. Interestingly, these effects have opposing and incongruent consequences on the progression and severity of the disease. We observed that inhibition of APC increased BBB permeability as evidenced by considerable leukocyte infiltration in the brains of anti-PC mice. However, APC depletion also had profound effects on the inflammatory responses of various leukocyte populations, resulting in increased and

more activated $CD11b^+$ myeloid population, including the MDSC subset, which is suppressive to the effector T-cells required for disease progression. Consequently, the net effect of APC inhibition in EAE is attenuated disease.

The ability of APC to influence inflammatory conditions has been largely attributed to its cell signaling capabilities (1–3). APC is known to regulate the functions of various cell types including several leukocyte populations. The cellular receptors that are involved in APC-mediated signaling in leukocytes, however, is still unclear. In endothelial cells, APC controls cellular processes by interacting with EPCR, a receptor which localizes APC on the cell surface and within the lipid rafts of the cell membrane, allowing APC to activate PAR-1 and initiate various cell signaling cascades (5, 7). Several studies, however, have shown that APC's effects on myeloid cells are not dependent on EPCR and may involve other cellular receptors (42, 43, 45). A recent study by Cao *et. al.* has identified the CD11b integrin as the facilitator of APC's anti-inflammatory effects on macrophages (15). The group demonstrated that APC can effectively inhibit the pro-inflammatory responses of macrophages, including the down-regulation of iNOS, STAT3, and NF-κB expression, through APC's interaction with CD11b on the cell surface (15). They propose that CD11b expressed on leukocytes serves a similar function as EPCR on endothelial cells; specifically, CD11b binds APC and co-localizes it with PAR-1 within the lipid rafts of the cell membrane, thereby facilitating PAR-1 activation and resulting in the down-regulation of inflammatory signaling cascades (15).

In our study, we observed that inhibition of APC during EAE resulted in the significant increase in various $CD11b^+$ populations. Since APC has been shown to be a direct negative regulator of $CD11b^+$ cells, we hypothesize that inhibition of APC during EAE likely resulted in the increased and more activated $CD11b^+$ subsets. Further, we propose that certain suppressive $CD11b^+$ populations, notably MDSCs, expanded as a result of APC inhibition, culminating in the attenuated disease observed in anti-PC mice.

MDSCs are a heterogenous population of immature myeloid cells characterized as potent T-cell suppressors (29, 39, 40). In mice, MDSCs are identified by cell surface co-expression of CD11b and Gr-1 (29). Antibodies to Gr-1 bind two epitopes, Ly6C and Ly6G. MDSCs are categorized into two subsets based on the cell surface expression of these two molecules (29, 39, 40). The $CD11b^+Ly6C^{hi}Ly6G^+$ subset has a monocytic morphology while the $CD11b^+Ly6C^{low}Ly6G^-$ subset is granulocytic (29, 39, 40). Since both MDSC subsets express Ly6C, we utilized the co-expression of CD11b and Ly6C as identifying markers for MDSCs. Thus, the MDSC population identified in our study incorporates both subsets. The immunoregulatory effects of MDSCs on T-cells have initially been described in tumor micro-environments, but recent studies have also reported the presence of MDSCs in various pathological settings, including parasitic infections and autoimmunity (40). The suppressive capacities of these cells have been specifically observed in EAE. $CD11b^+LyC^{high}$ cells increased in the spleen following EAE induction, and these cells are capable of suppressing the proliferation of $CD4^+$ and $CD8^+$ T-cells (46). In another study, MDSCs were observed in the spinal cord (SC) during EAE where they promote T-cell apoptosis (47). Consistent with these studies, we observed that anti-PC mice with attenuated EAE have increased splenic $CD11b^+Ly6C^+$ cells. Moreover, we observed that the frequency and the proliferative capacity of $CD4^+$ T-cells are significantly reduced in these mice, consistent with the known suppressive effects of MDSCs on T-cell proliferation. We also observed that the proliferation of $MOG_{35–55}$-specific T-cells is inhibited when co-cultured with $CD11b^+$ cells from anti-PC mice, confirming the direct suppressive effects of the $CD11b^+$ population on antigen-induced T-cell proliferation. The mechanisms utilized by monocytic MDSCs to suppress T-cell proliferation involve Arg I activity and /or the production of NO (29). Increased Arg I activity depletes L-arginine from the microenvironment, consequently

inhibiting both T-cell cycle progression (48) and CD3 expression (49). Similarly, increased production of NO limits T-cell proliferation by inhibiting the IL-2 receptor downstream pathway (50). The suppressive capability of granulocytic MDSCs has been attributed to the generation of ROS, which suppresses antigen-induced T-cell proliferation (29, 39). Accordingly, we observed increased Arg I activity in splenocytes and significantly higher expression of iNOS and ROS generation in $CD11b^+Ly6C^+$ cells in anti-APC mice, confirming the increased activation of the suppressive MDSC population in these mice.

Several studies have demonstrated that MDSCs exhibit the capacity to induce the generation of T-regs (51, 52). The accumulation of T-regs within the tumor microenvironment has been associated to MDSCs (52), and *in vitro* studies have confirmed that MDSCs co-cultured with T-cells results in T-reg expansion (51). The mechanism through which MDSCs induce T-reg expansion has yet to be elucidated; interestingly Arg I activity in MDSCs has been implicated in T-reg generation (53). We observed that the expansion of $CD11b^+Ly6C^+$ population in anti-PC mice was accompanied by an increase in T-reg subset, both in the CNS and in the periphery. We further showed that co-culture of $CD4^+$ T-cells with $CD11b^+$ cells from anti-APC mice increased T-reg frequency. These findings further exhibit the suppressive capability of $CD11b^+$ cells from anti-PC mice, not only via direct suppression of T-cell function but also through induction of T-regs.

MDSCs are known to expand in various pathogenic and inflammatory conditions, including during EAE (39, 40). We postulate that inhibition of APC contributed to the further accumulation and activation of these cells as EAE progressed. It has been widely proposed that the expansion and cell survival of MDSCs in pathogenic conditions are regulated by the transcription factor, Stat-3 (44, 54, 55). Inhibition of Stat3 signaling *in vivo* abrogated the expansion of MDSCs in tumor-bearing mice (55). Stat-3 expression in MDSCs has been known to drive cell survival by up-regulating anti-apoptotic genes (39). Accordingly, we observed increased Stat3 expression and Stat3 activation in $CD11b^+Ly6C^+$ cells in anti-PC mice, coupled with decreased apoptosis in these cells. Moreover, the suppressive activities of MDSCs, specifically the generation of ROS, are also reportedly regulated by Stat3 (29). One likely mechanism through which APC inhibition affected the increase in MDSC numbers and the suppressive activities of these cells is through APC's regulatory capability to suppress Stat3 expression. In the study by Cao et. al, APC has been demonstrated to specifically suppress the expression of Stat3 in myeloid cells through engagement with the CD11b integrin (15). Furthermore, APC is known to regulate the expression and nuclear translocation of NF-κB, which is also central in regulating the immunosuppressive capabilities of MDSCs (29). Based on these studies, we postulate that APC is a negative regulator of MDSCs, likely by binding the CD11b integrin and down-regulating Stat-3 and/or NF-κB signaling. Therefore, it follows that inhibition of APC results in the increased activation of Stat-3 and/or NF-κB in MDSCs, culminating in the increased expansion and activation of this leukocyte subset.

The influence of APC on inflammatory settings can be mediated at two different fronts, namely APC's direct effects on leukocytes and on vascular barrier permeability (3). Consistently, we observed that inhibition of APC during EAE not only affected leukocyte function but additionally increased BBB permeability, as evidenced by considerable leukocyte infiltration in the brains of anti-PC mice and the extensive perivascular cuffing observed in the brain parenchyma of these mice. Despite exhibiting attenuated clinical symptoms, anti-PC mice had heavy cellular infiltrates in the brain, and the degree of infiltration is comparable to control mice with severe clinical symptoms. Interestingly, cellular infiltration in the SC of anti-PC mice was less pronounced. This deviates from the known pattern in classical EAE models, which is characterized by predominant infiltration and pathology in the SC (56, 57). The reason for the disparity in infiltration between the two

sites is unclear. It should be noted, however, that there are reported molecular differences governing leukocyte trafficking events in the brain and in the SC (58). Thus, it is likely that modulation of APC in the circulation can have separate and varying effects on leukocyte extravasation in the brain and SC, accounting for the observed disparity in cellular infiltration between the two sites.

Despite considerable leukocyte infiltration in the brain, the pathological condition in the CNS of anti-APC mice, specifically demyelination and microglial activation, is minimal compared to controls, and it follows that these mice exhibited attenuated clinical signs. This is an indication that the infiltrating population in the CNS of anti-PC mice is less inflammatory. In fact, we observed increased T-reg frequency in the CNS of these mice, as well as increased production of anti-inflammatory cytokine, IL-10, from cellular infiltrates. Further, we detected decreased pathogenic cytokines in the brains of anti-PC mice, specifically IFN-γ and IL-17, the signature cytokines produced by encephalitogenic $CD4^+$ T-cell subsets in EAE (25). We postulate that the decreased encephalitogenic $CD4^+$ T-cells in the CNS of anti-PC mice is a consequence of increased expansion of MDSCs in the periphery, which we have shown can effectively suppress the effector responses of $CD4^+$ T-cells, notably $MOG_{35–55}$-induced proliferation of $CD4^+$ T-cells, while concurrently inducing T-reg expansion.

Our findings demonstrate the complex and multi-faceted effects of APC inhibition on the EAE inflammatory setting, affecting both vascular permeability and leukocyte function, ultimately resulting in pathogenic conditions that have opposing overall influences on the progression of EAE. In addition, the effect of APC inhibition on the final outcome of EAE progression is likely dependent on the specific stage of the disease in which APC is inhibited. We inhibited APC during the induction stage of EAE. Therefore the effects of APC inhibition specifically influenced the initial activation and functional responses of leukocyte populations in the periphery, culminating into an increased and more activated myeloid subset while the effector $CD4^+$ T effector cells are diminished and suppressed. Inhibiting APC after disease onset, however, did not attenuate disease but actually resulted in a slightly increased disease severity (Sup. Fig. 3A). We postulate that at this point, the effector T-cells have sufficiently proliferated and have already infiltrated the CNS; therefore APC inhibition in the periphery, at this stage, would not profoundly affect the T-cell response. We attribute the slight increase in disease severity to the effects of APC inhibition on increased BBB permeability, further increasing the infiltration of pathogenic leukocytes (Sup. Fig. 3B) into the CNS. These findings demonstrate that the overall outcome of APC modulation in disease settings can be governed by a number of factors, including the specific stage of the disease.

In summary, APC inhibition during induction of EAE affected EAE pathogenesis at multiple fronts, specifically increasing BBB permeability and inducing a more activated $CD11b^+$ myeloid population, including the MDSC subset known to be potent T-cell suppressors. Since EAE is a pre-dominantly T-cell mediated disease, the net effect of APC depletion during EAE is alleviated disease severity. APC's influence on the MDSC population is presented here for the first time. The ability of APC to affect the functional responses of MDSCs opens a novel therapeutic avenue through which APC can influence disease conditions. MDSCs, for instance, are widely-reported to be a major hindrance in tumor immunity. The findings in this study, which suggests that APC can negatively regulate MDSCs, bring to the fore, the possible therapeutic relevance of APC in cancer immunotherapies. Overall, these findings present a novel influence of APC on the immune response and contribute to further elucidating the complex interaction between the immune and coagulation systems.

Supplementary Material

Refer to Web version on PubMed Central for supplementary material.

References

1. Esmon CT. Protein C anticoagulant system--anti-inflammatory effects. Semin Immunopathol. 2012; 34:127–132. [PubMed: 21822632]
2. Weiler H. Regulation of inflammation by the protein C system. Crit Care Med. 2010; 38:S18–S25. [PubMed: 20083909]
3. Mosnier LO, Zlokovic BV, Griffin JH. The cytoprotective protein C pathway. Blood. 2007; 109:3161–3172. [PubMed: 17110453]
4. Van de Wouwer M, Collen D, Conway EM. Thrombomodulin-protein C-EPCR system: integrated to regulate coagulation and inflammation. Arterioscler Thromb Vasc Biol. 2004; 24:1374–1383. [PubMed: 15178554]
5. Niessen F, Furlan-Freguia C, Fernandez JA, Mosnier LO, Castellino FJ, Weiler H, Rosen H, Griffin JH, Ruf W. Endogenous EPCR/aPC-PAR1 signaling prevents inflammation-induced vascular leakage and lethality. Blood. 2009; 113:2859–2866. [PubMed: 19141861]
6. Feistritzer C, Riewald M. Endothelial barrier protection by activated protein C through PAR1-dependent sphingosine 1-phosphate receptor-1 crossactivation. Blood. 2005; 105:3178–3184. [PubMed: 15626732]
7. Van Sluis GL, Niers TM, Esmon CT, Tigchelaar W, Richel DJ, Buller HR, Van Noorden CJ, Spek CA. Endogenous activated protein C limits cancer cell extravasation through sphingosine-1-phosphate receptor 1-mediated vascular endothelial barrier enhancement. Blood. 2009; 114:1968–1973. [PubMed: 19571314]
8. Pereira CP, Bachli EB, Schaer DJ, Schoedon G. Transcriptome analysis revealed unique genes as targets for the anti-inflammatory action of activated protein C in human macrophages. PLoS One. 2010; 5:e15352. [PubMed: 20976180]
9. Pereira C, Schaer DJ, Bachli EB, Kurrer MO, Schoedon G. Wnt5A/CaMKII signaling contributes to the inflammatory response of macrophages and is a target for the antiinflammatory action of activated protein C and interleukin-10. Arterioscler Thromb Vasc Biol. 2008; 28:504–510. [PubMed: 18174455]
10. White B, Schmidt M, Murphy C, Livingstone W, O'Toole D, Lawler M, O'Neill L, Kelleher D, Schwarz HP, Smith OP. Activated protein C inhibits lipopolysaccharide-induced nuclear translocation of nuclear factor kappaB (NF-kappaB) and tumour necrosis factor alpha (TNF-alpha) production in the THP-1 monocytic cell line. Br J Haematol. 2000; 110:130–134. [PubMed: 10930989]
11. Yuksel M, Okajima K, Uchiba M, Horiuchi S, Okabe H. Activated protein C inhibits lipopolysaccharide-induced tumor necrosis factor-alpha production by inhibiting activation of both nuclear factor-kappa B and activator protein-1 in human monocytes. Thromb Haemost. 2002; 88:267–273. [PubMed: 12195699]
12. Joyce DE, Gelbert L, Ciaccia A, DeHoff B, Grinnell BW. Gene expression profile of antithrombotic protein c defines new mechanisms modulating inflammation and apoptosis. J Biol Chem. 2001; 276:11199–11203. [PubMed: 11278252]
13. Stephenson DA, Toltl LJ, Beaudin S, Liaw PC. Modulation of monocyte function by activated protein C, a natural anticoagulant. J Immunol. 2006; 177:2115–2122. [PubMed: 16887970]
14. Shua F, Kobayashia H, Fukudomeb K, Tsuneyoshib N, Kimotob M, Teraoa T. Activated protein C suppresses tissue factor expression on U937 cells in the endothelial protein C receptor-dependent manner. FEBS Lett. 2000; 477:208–212. [PubMed: 10908722]
15. Cao C, Gao Y, Li Y, Antalis TM, Castellino FJ, Zhang L. The efficacy of activated protein C in murine endotoxemia is dependent on integrin CD11b. J Clin Invest. 2010; 120:1971–1980. [PubMed: 20458145]

16. Bernard GR, Vincent JL, Laterre PF, LaRosa SP, Dhainaut JF, Lopez-Rodriguez A, Steingrub JS, Garber GE, Helterbrand JD, Ely EW, Fisher CJ Jr. Efficacy and safety of recombinant human activated protein C for severe sepsis. N Engl J Med. 2001; 344:699–709. [PubMed: 11236773]
17. Ranieri VM, Thompson BT, Barie PS, Dhainaut JF, Douglas IS, Finfer S, Gardlund B, Marshall JC, Rhodes A, Artigas A, Payen D, Tenhunen J, Al-Khalidi HR, Thompson V, Janes J, Macias WL, Vangerow B, Williams MD. Drotrecogin alfa (activated) in adults with septic shock. N Engl J Med. 2012; 366:2055–2064. [PubMed: 22616830]
18. Vincent JL. The rise and fall of drotrecogin alfa (activated). The Lancet infectious diseases. 2012
19. Shibata M, Kumar SR, Amar A, Fernandez JA, Hofman F, Griffin JH, Zlokovic BV. Anti-inflammatory, antithrombotic, and neuroprotective effects of activated protein C in a murine model of focal ischemic stroke. Circulation. 2001; 103:1799–1805. [PubMed: 11282913]
20. Zhong Z, Ilieva H, Hallagan L, Bell R, Singh I, Paquette N, Thiyagarajan M, Deane R, Fernandez JA, Lane S, Zlokovic AB, Liu T, Griffin JH, Chow N, Castellino FJ, Stojanovic K, Cleveland DW, Zlokovic BV. Activated protein C therapy slows ALS-like disease in mice by transcriptionally inhibiting SOD1 in motor neurons and microglia cells. J Clin Invest. 2009; 119:3437–3449. [PubMed: 19841542]
21. Scaldaferri F, Sans M, Vetrano S, Graziani C, De Cristofaro R, Gerlitz B, Repici A, Arena V, Malesci A, Panes J, Grinnell BW, Danese S. Crucial role of the protein C pathway in governing microvascular inflammation in inflammatory bowel disease. J Clin Invest. 2007; 117:1951–1960. [PubMed: 17557119]
22. Yasui H, Gabazza EC, Tamaki S, Kobayashi T, Hataji O, Yuda H, Shimizu S, Suzuki K, Adachi Y, Taguchi O. Intratracheal administration of activated protein C inhibits bleomycin-induced lung fibrosis in the mouse. Am J Respir Crit Care Med. 2001; 163:1660–1668. [PubMed: 11401891]
23. McFarland HF, Martin R. Multiple sclerosis: a complicated picture of autoimmunity. Nat Immunol. 2007; 8:913–919. [PubMed: 17712344]
24. Gold R, Linington C, Lassmann H. Understanding pathogenesis and therapy of multiple sclerosis via animal models: 70 years of merits and culprits in experimental autoimmune encephalomyelitis research. Brain. 2006; 129:1953–1971. [PubMed: 16632554]
25. Batoulis H, Addicks K, Kuerten S. Emerging concepts in autoimmune encephalomyelitis beyond the CD4/T(H)1 paradigm. Ann Anat. 2010; 192:179–193. [PubMed: 20692821]
26. Han MH, Hwang SI, Roy DB, Lundgren DH, Price JV, Ousman SS, Fernald GH, Gerlitz B, Robinson WH, Baranzini SE, Grinnell BW, Raine CS, Sobel RA, Han DK, Steinman L. Proteomic analysis of active multiple sclerosis lesions reveals therapeutic targets. Nature. 2008; 451:1076–1081. [PubMed: 18278032]
27. Koh CS, Gausas J, Paterson PY. Neurovascular permeability and fibrin deposition in the central neuraxis of Lewis rats with cell-transferred experimental allergic encephalomyelitis in relationship to clinical and histopathological features of the disease. Journal of neuroimmunology. 1993; 47:141–145. [PubMed: 8370766]
28. Inaba Y, Ichikawa M, Inoue A, Itoh M, Kyogashima M, Sekiguchi Y, Nakamura S, Komiyama A, Koh C. Plasma thrombin-antithrombin III complex is associated with the severity of experimental autoimmune encephalomyelitis. J Neurol Sci. 2001; 185:89–93. [PubMed: 11311288]
29. Condamine T, Gabrilovich DI. Molecular mechanisms regulating myeloid-derived suppressor cell differentiation and function. Trends Immunol. 2011; 32:19–25. [PubMed: 21067974]
30. Xu J, Ji Y, Zhang X, Drake M, Esmon CT. Endogenous activated protein C signaling is critical to protection of mice from lipopolysaccaride-induced septic shock. J Thromb Haemost. 2009; 7:851–856. [PubMed: 19320827]
31. Corraliza IM, Campo ML, Soler G, Modolell M. Determination of arginase activity in macrophages: a micromethod. Journal of immunological methods. 1994; 174:231–235. [PubMed: 8083527]
32. Grisham MB, Yamada T. Neutrophils, nitrogen oxides, and inflammatory bowel disease. Annals of the New York Academy of Sciences. 1992; 664:103–115. [PubMed: 1456643]
33. Gareau PJ, Wymore AC, Cofer GP, Johnson GA. Imaging inflammation: direct visualization of perivascular cuffing in EAE by magnetic resonance microscopy. J Magn Reson Imaging. 2002; 16:28–36. [PubMed: 12112500]

34. Sabat R, Grutz G, Warszawska K, Kirsch S, Witte E, Wolk K, Geginat J. Biology of interleukin-10. Cytokine Growth Factor Rev. 2010; 21:331–344. [PubMed: 21115385]
35. Brown DA, Sawchenko PE. Time course and distribution of inflammatory and neurodegenerative events suggest structural bases for the pathogenesis of experimental autoimmune encephalomyelitis. J Comp Neurol. 2007; 502:236–260. [PubMed: 17348011]
36. Mills JH, Kim DG, Krenz A, Chen JF, Bynoe MS. A2A adenosine receptor signaling in lymphocytes and the central nervous system regulates inflammation during experimental autoimmune encephalomyelitis. J Immunol. 2012; 188:5713–5722. [PubMed: 22529293]
37. Ercolini AM, Miller SD. Mechanisms of immunopathology in murine models of central nervous system demyelinating disease. J Immunol. 2006; 176:3293–3298. [PubMed: 16517694]
38. Montero AJ, Diaz-Montero CM, Kyriakopoulos CE, Bronte V, Mandruzzato S. Myeloid-derived suppressor cells in cancer patients: a clinical perspective. J Immunother. 2012; 35:107–115. [PubMed: 22306898]
39. Gabrilovich DI, Nagaraj S. Myeloid-derived suppressor cells as regulators of the immune system. Nat Rev Immunol. 2009; 9:162–174. [PubMed: 19197294]
40. Cripps JG, Gorham JD. MDSC in autoimmunity. Int Immunopharmacol. 2011; 11:789–793. [PubMed: 21310255]
41. Zea AH, Rodriguez PC, Culotta KS, Hernandez CP, DeSalvo J, Ochoa JB, Park HJ, Zabaleta J, Ochoa AC. L-Arginine modulates CD3zeta expression and T cell function in activated human T lymphocytes. Cell Immunol. 2004; 232:21–31. [PubMed: 15922712]
42. O'Brien LA, Richardson MA, Mehrbod SF, Berg DT, Gerlitz B, Gupta A, Grinnell BW. Activated protein C decreases tumor necrosis factor related apoptosis-inducing ligand by an EPCR-independent mechanism involving Egr-1/Erk-1/2 activation. Arterioscler Thromb Vasc Biol. 2007; 27:2634–2641. [PubMed: 17932312]
43. Toltl LJ, Beaudin S, Liaw PC. Activated protein C up-regulates IL-10 and inhibits tissue factor in blood monocytes. J Immunol. 2008; 181:2165–2173. [PubMed: 18641355]
44. Sonda N, Chioda M, Zilio S, Simonato F, Bronte V. Transcription factors in myeloid-derived suppressor cell recruitment and function. Curr Opin Immunol. 2011; 23:279–285. [PubMed: 21227670]
45. Yang XV, Banerjee Y, Fernandez JA, Deguchi H, Xu X, Mosnier LO, Urbanus RT, de Groot PG, White-Adams TC, McCarty OJ, Griffin JH. Activated protein C ligation of ApoER2 (LRP8) causes Dab1-dependent signaling in U937 cells. Proc Natl Acad Sci U S A. 2009; 106:274–279. [PubMed: 19116273]
46. Zhu B, Bando Y, Xiao S, Yang K, Anderson AC, Kuchroo VK, Khoury SJ. CD11b+Ly-6C(hi) suppressive monocytes in experimental autoimmune encephalomyelitis. J Immunol. 2007; 179:5228–5237. [PubMed: 17911608]
47. Moline-Velazquez V, Cuervo H, Vila-Del Sol V, Ortega MC, Clemente D, de Castro F. Myeloid-derived suppressor cells limit the inflammation by promoting T lymphocyte apoptosis in the spinal cord of a murine model of multiple sclerosis. Brain Pathol. 2011; 21:678–691. [PubMed: 21507122]
48. Rodriguez PC, Quiceno DG, Ochoa AC. L-arginine availability regulates T-lymphocyte cell-cycle progression. Blood. 2007; 109:1568–1573. [PubMed: 17023580]
49. Rodriguez PC, Zea AH, DeSalvo J, Culotta KS, Zabaleta J, Quiceno DG, Ochoa JB, Ochoa AC. L-arginine consumption by macrophages modulates the expression of CD3 zeta chain in T lymphocytes. J Immunol. 2003; 171:1232–1239. [PubMed: 12874210]
50. Bingisser RM, Tilbrook PA, Holt PG, Kees UR. Macrophage-derived nitric oxide regulates T cell activation via reversible disruption of the Jak3/STAT5 signaling pathway. J Immunol. 1998; 160:5729–5734. [PubMed: 9637481]
51. Hoechst B, Ormandy LA, Ballmaier M, Lehner F, Kruger C, Manns MP, Greten TF, Korangy F. A new population of myeloid-derived suppressor cells in hepatocellular carcinoma patients induces CD4(+)CD25(+)Foxp3(+) T cells. Gastroenterology. 2008; 135:234–243. [PubMed: 18485901]
52. Huang B, Pan PY, Li Q, Sato AI, Levy DE, Bromberg J, Divino CM, Chen SH. Gr-1+CD115+ immature myeloid suppressor cells mediate the development of tumor-induced T regulatory cells and T-cell anergy in tumor-bearing host. Cancer Res. 2006; 66:1123–1131. [PubMed: 16424049]

53. Serafini P, Mgebroff S, Noonan K, Borrello I. Myeloid-derived suppressor cells promote cross-tolerance in B-cell lymphoma by expanding regulatory T cells. Cancer Res. 2008; 68:5439–5449. [PubMed: 18593947]

54. Chalmin F, Ladoire S, Mignot G, Vincent J, Bruchard M, Remy-Martin JP, Boireau W, Rouleau A, Simon B, Lanneau D, De Thonel A, Multhoff G, Hamman A, Martin F, Chauffert B, Solary E, Zitvogel L, Garrido C, Ryffel B, Borg C, Apetoh L, Rebe C, Ghiringhelli F. Membrane-associated Hsp72 from tumor-derived exosomes mediates STAT3-dependent immunosuppressive function of mouse and human myeloid-derived suppressor cells. J Clin Invest. 2010; 120:457–471. [PubMed: 20093776]

55. Wu L, Du H, Li Y, Qu P, Yan C. Signal transducer and activator of transcription 3 (Stat3C) promotes myeloid-derived suppressor cell expansion and immune suppression during lung tumorigenesis. Am J Pathol. 2011; 179:2131–2141. [PubMed: 21864492]

56. Kuerten S, Lehmann PV. The immune pathogenesis of experimental autoimmune encephalomyelitis: lessons learned for multiple sclerosis? J Interferon Cytokine Res. 2011; 31:907–916. [PubMed: 21936633]

57. Recks MS, Addicks K, Kuerten S. Spinal cord histopathology of MOG peptide 35–55-induced experimental autoimmune encephalomyelitis is time- and score-dependent. Neurosci Lett. 2011; 494:227–231. [PubMed: 21406210]

58. Vajkoczy P, Laschinger M, Engelhardt B. Alpha4-integrin-VCAM-1 binding mediates G protein-independent capture of encephalitogenic T cell blasts to CNS white matter microvessels. J Clin Invest. 2001; 108:557–565. [PubMed: 11518729]

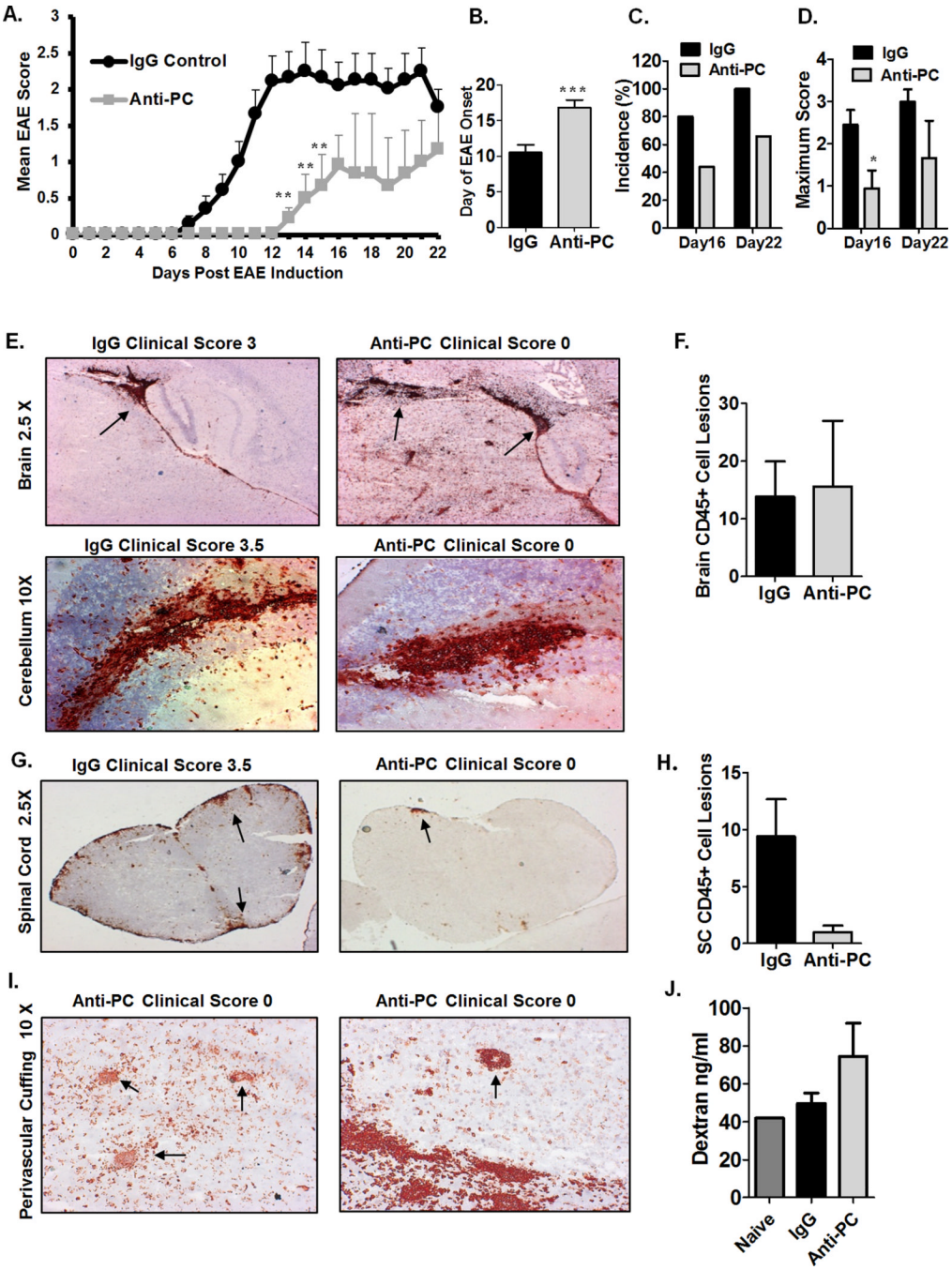

Figure 1. Mice treated with anti-PC exhibit attenuated EAE despite considerable cellular infiltration in the brain

(A) To induce EAE, BL/6 mice were immunized with $MOG_{35–55}$ in CFA; pertussis toxin was i.v. injected on the day of immunization and 48 hours later. Anti-PC or IgG was i.p. injected on days 0, 2, 4, and 6 post EAE induction. Mice were monitored daily to assess clinical signs, and scores were assigned based on the scoring system outlined in materials and methods. Scores were plotted as the mean ± S.E.M (anti-PC n = 9, IgG control n = 10. On day 16, mice from both groups were randomly selected for tissue collection. ** $p < 0.01$ by Mann Whitney test; Statistical analysis up to day 16 included all mice. Statistical analysis up to day 22 did not include mice taken for tissue collection on day 16). The results shown

are representative of five independent experiments. (**B)** Day of EAE onset for each mouse from both IgG or Anti-PC group are averaged and shown with ± SEM (*** $p < 0.001$ by Student *t* test). For mice that were not showing clinical signs at the time of tissue collection, the day following tissue collection was assigned as the day of onset. (**C)** EAE incidence on days 16 and 22 post EAE induction is represented as percentages. The calculated incidence on Day 22 does not include the mice that were taken for tissue collection on day 16. (**D)** Maximum clinical score reached by each mouse from both groups were averaged and represented with ± SEM (* $p < 0.05$ by Student *t* test). (**E)** Brains from both groups were harvested at the peak of disease (days 14–17) following EAE induction. Brain sections were stained with anti-CD45 (red). Arrows indicate $CD45^+$ cell aggregates in brain sections. Images were captured using using a Zeiss Axio Imager M1 microscope. (**F**) $CD45^+$ cell aggregates in brain sections of mice from both groups were individually counted at 10X magnification using a Zeiss Axio Imager M1 microscope. Counts are represented as means ± SEM (IgG n = 6, anti-PC n = 5). **(G)** Spinal cords from IgG or anti-PC mice were harvested at days 14–17 following EAE induction. Spinal cord sections were stained with anti-CD45 (red). Arrows indicate $CD45^+$ cell aggregates. Images were captured using using a Zeiss Axio Imager M1 microscope. (**H**) $CD45^+$ cell aggregates in spinal cord sections of mice from both groups were individually counted at 10X magnification using a Zeiss Axio Imager M1 microscope. Counts are shown as means ± SEM (IgG n = 6, anti-PC n = 5). (**I)** Brain sections were analyzed for $CD45^+$ cellular infiltrates surrounding blood vessels in the brain parenchyma of anti-PC mice. Images were captured using using a Zeiss Axio Imager M1 microscope. (**J)** At day 5 post EAE induction, fluorescent dextran molecules (2 mg) were i.v. injected into the systemic circulation of anti-pc and IgG mice. Brains were harvested 5 hours later to assess the degree of dextran extravasation. The concentration of extravasated dextran in brain homogenates was determined based on a standard curve. Data shown as means ± SEM (IgG n = 3, anti-PC n = 2). The experiment was repeated twice with the same result.

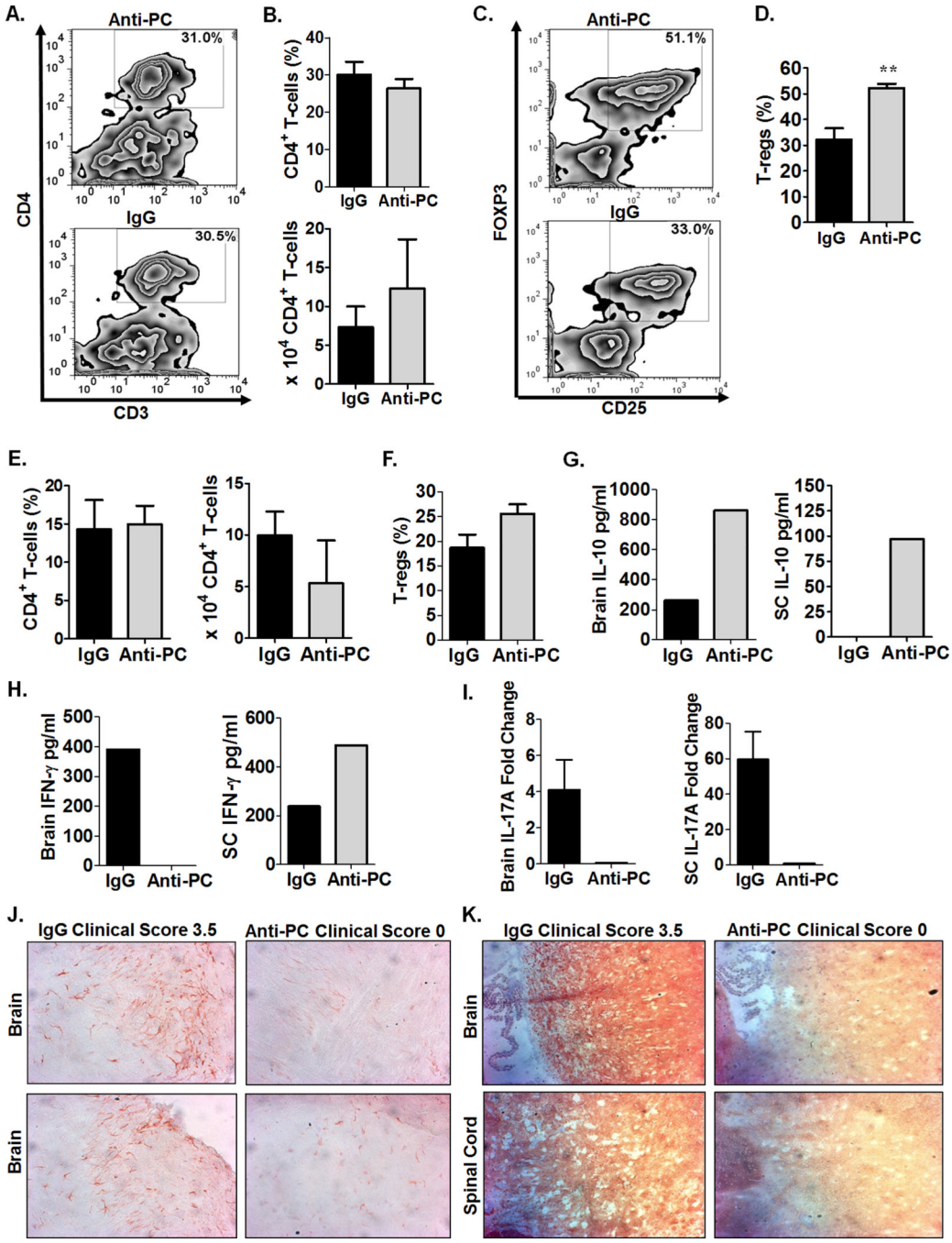

Figure 2. Anti-PC mice exhibit reduced pathogenic and inflammatory conditions in the CNS

A) At day 17 following EAE induction, cellular infiltrates from brains of anti-PC and IgG mice were isolated by percoll gradient, and cells were subjected to flow cytometry analysis to assess the frequency of $CD4^+$ T-cells among $CD45^{high}$ cells. Data are shown as flow cytometric contour plot gated on $CD45^{high}$ cells. (**B**) $CD4^+$ T-cell frequencies in the brains from both groups are represented as means ± SEM on the upper panel, and $CD4^+$ T-cell absolute cell counts are shown as means ± SEM on the lower panel (IgG n = 4, anti-PC n = 3). (**C**) The frequency of T-regs ($CD25^+$, $Foxp3^+$) among $CD4^+$ T-cell infiltrates in the brain was assessed by flow cytometry. Data are shown as flow cytometric contour plot gated on

$CD4^+$ cells. (**D)** Frequencies of T-regs in the brains from both groups are shown as means + SEM. (Control n = 6, anti-PC n = 4, ** $p < 0.01$ by Student *t* test). (**E)** Leukocyte infiltrates from the spinal cords of anti-PC mice and controls were isolated by percoll gradient and assessed for the frequency of $CD4^+$ T-cells among $CD45^{high}$ cells. Frequencies (left panel) and absolute cell counts (right panel) of CD4 T-cells are shown as means ± SEM (IgG n = 4, anti-PC n = 3). (**F)** T-regs among $CD4^+$ T-cells in the spinal cord at day 16 following EAE induction. Data are represented as means ± SEM (n = 5–6). (**G-H**) CNS infiltrates from both anti-PC and control mice were isolated as described above. Cells from individual mouse (n < 3) were pooled for each group and re-stimulated with $MOG_{35–55}$ *in vitro*. After 48 hours, supernatants were collected and the production of (**G)** IL-10 and (**H)** IFN-γ were measured by ELISA. **I)** Brains and SC from both groups (n = 3) were homogenized, and whole-cell mRNA was isolated using the Trizol-based extraction process. IL-17A mRNA was quantified using real-time quantitative PCR, and expression levels were calculated using the $2^{-\Delta\Delta Ct}$ method. The expression levels of IL-17A were normalized to the internal control gene, GAPDH. IL-17A expression is represented as fold change in expression relative to naïve mice (non-EAE induced). (**J)** Brains were harvested at the peak of disease (days 14–17) following EAE induction. Brain sections from IgG and anti-PC mice were stained with anti-Iba-1 (red) to assess microglial activation. Arrows indicate pronounced Iba-1 staining. (**K)** CNS sections were examined for severity of demyelination by staining with anti-MOG antibody. Areas in the CNS that do not positively stain for MOG denote demyelination as indicated by arrows.

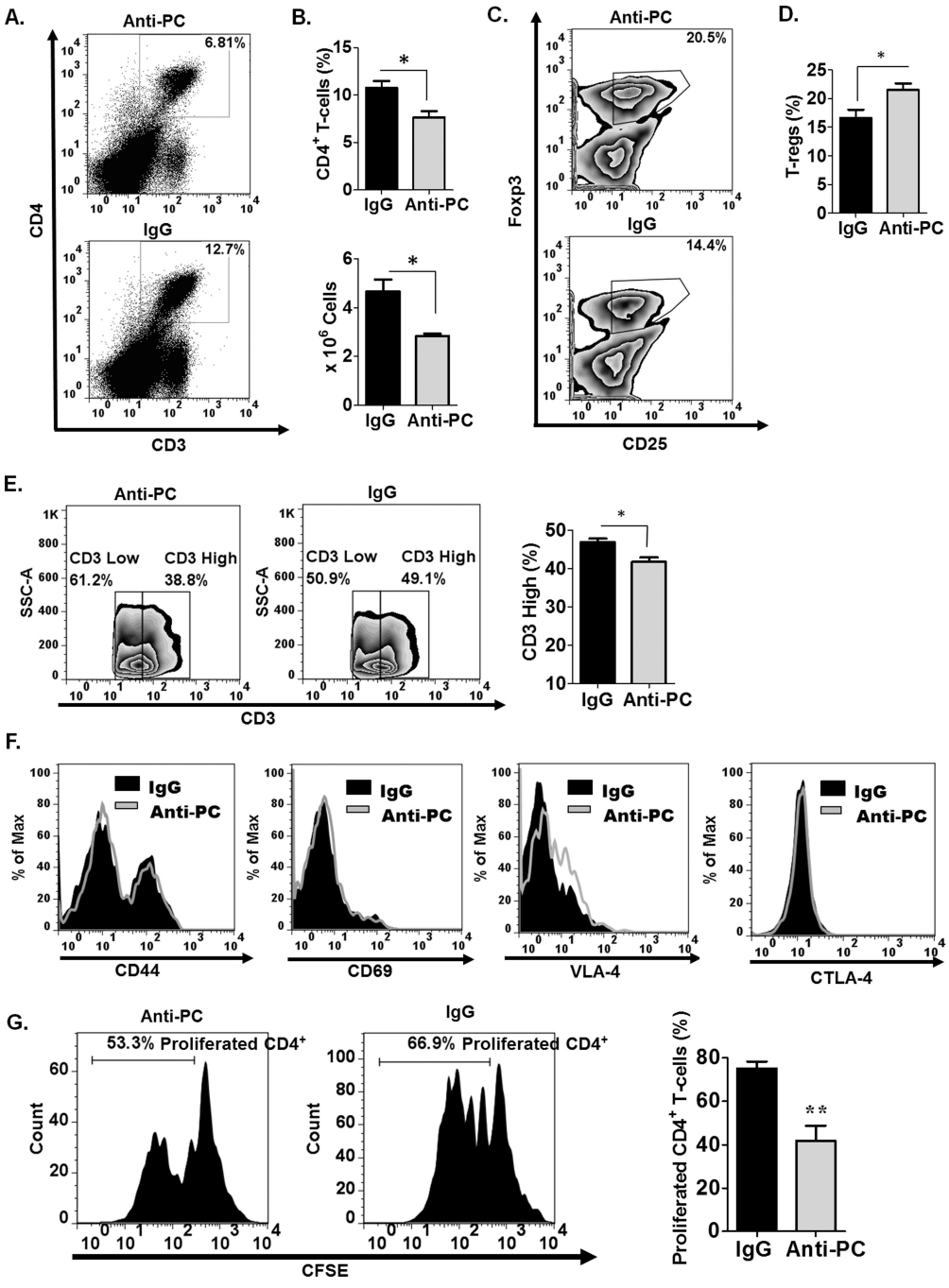

Figure 3. Peripheral CD4$^+$ T-cells in anti-PC mice are significantly decreased and functionally deficient

(A) The frequency of splenic CD4 $^+$ T-cells from anti-PC and control mice was examined by flow cytometry at day 17 following EAE induction. Data are represented as flow cytometric dot plots. (**B)** The upper panel shows the graphical representation of the mean percentage of splenic CD4$^+$ T-cells, and the lower panel shows the absolute cell counts of splenic CD4$^+$ T-cells, respectively. Data are represented as means ± SEM (control n = 6; anti-PC n = 4; * $p < 0.05$ by Student *t* test). (**C**) The frequency of splenic T-regs (CD4$^+$, CD25$^+$, Foxp3$^+$) among CD4$^+$ T-cells was assessed by flow cytometry. Data are shown as cytometric contour plots (gated on CD3$^+$CD4$^+$). (**D)** The percentages of T-regs among CD4$^+$ T-cells in the periphery

are shown as means ± SEM (control n = 6; anti-PC n = 4; * $p < 0.05$ by Student *t* test). (**E)** CD3 expression on splenic $CD4^+$ T-cells was assessed by flow cytometry. Data are shown as flow cytometric contour plot on the left (gated on $CD3^+$ cells), and right panel shows the percentage of $CD3^{high}$ splenocytes from both groups. Data are shown as means ± SEM (n > 3; * $p < 0.05$ by Student t test). (**F)** The cell surface expression of CD44, CD69, VLA-4 and CTLA-4 on splenic $CD4^+$ was assessed by flow cytometry. Expression levels are presented as histograms. **(G**) Splenocytes from control and anti-PC mice were labeled with CFSE and cultured *in vitro*. T-cells in whole splenocyte culture were stimulated with plate-bound anti-CD3 and soluble anti-CD28 for 96 hours. The proliferative capacity of $CD4^+$ T-cells was assessed by flow cytometry based on CFSE dilution. Left panels show the histogram representation of CFSE labeled $CD4^+$ T-cells from both experimental groups (gated on $CD4^+$ cells). Data on right panel are the graphical representation of the percentage of $CD4^+$ T-cells that have proliferated based on CFSE dilution. Data represented as means ± SEM (n=4; ** $p < 0.01$ by Student *t* test).

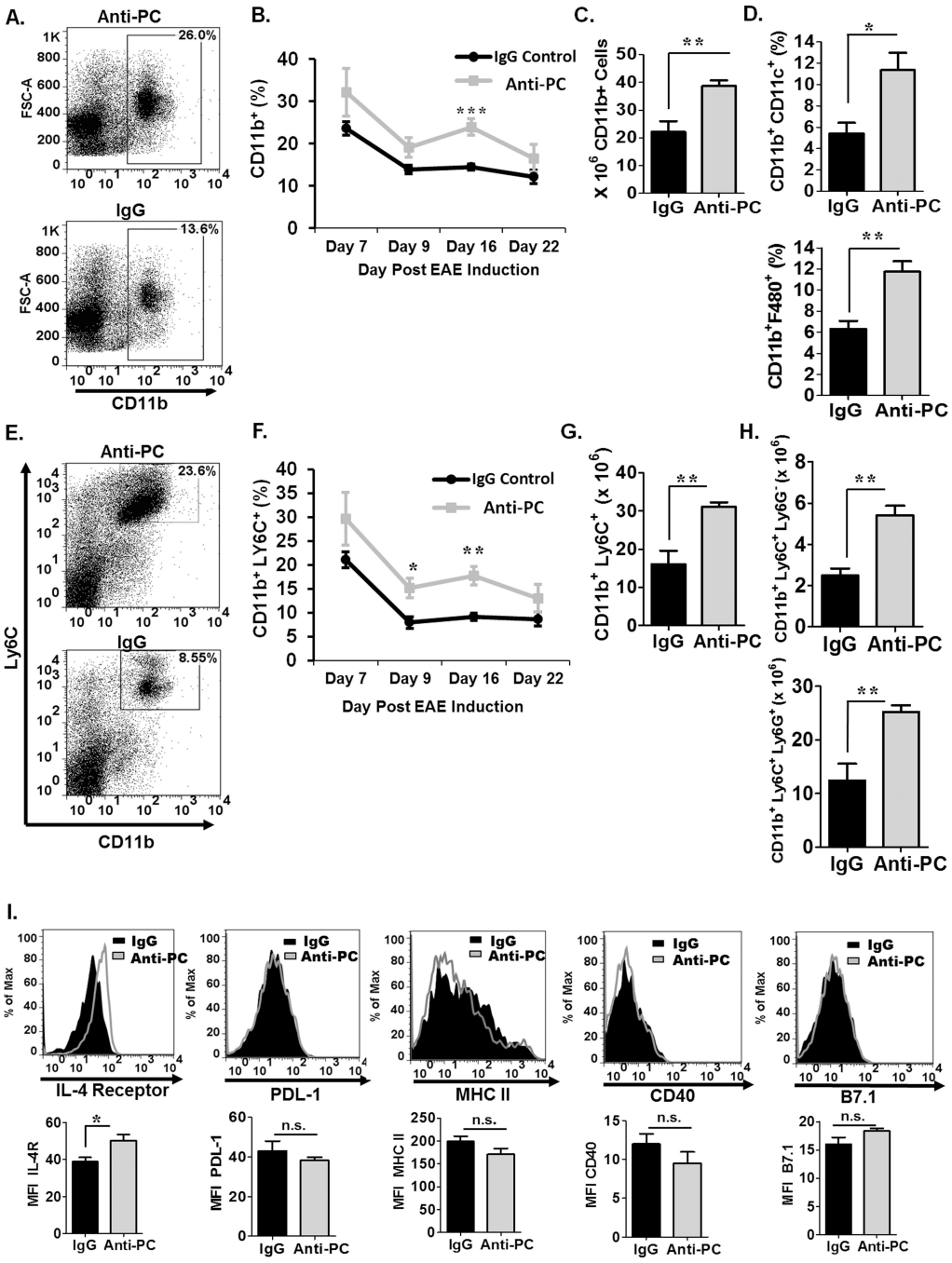

Figure 4. CD11b$^+$ cells in the periphery of anti-PC mice are significantly increased

(A) Splenocytes were harvested from the anti-PC and IgG mice at day 17 following EAE induction, and the frequency of CD11b$^+$ was assessed by flow cytometry. Data are presented as flow cytometric dot plots. (**B)** The frequency of splenic CD11b$^+$ cells in anti-PC or IgG mice at various stages of EAE progression was assessed by flow cytometry. Data are presented as means ± SEM (n > 3, ** p < 0.001 by Student *t* test). (**C)** The absolute cell counts of splenic CD11b$^+$ cells from both groups are presented as means ± SEM (n > 3, ** p < 0.01). (**D**) Splenocyte frequency of specific Cd11b $^+$ subsets, namely macrophages (CD11b+ F480+) (upper panel) and DC's (CD11b+ CD11c+) (bottom panel), was examined

by flow cytometry. Data are presented as means ± SEM (n > 3, p * < 0.05 * p < 0.001 by Student *t* test). (**E**) The frequency of splenic MDSCs was examined by staining for cell surface markers, CD11b and Ly6C. Frequencies were analyzed by flow cytometry. Data are represented as flow cytometric dot plots. (**F)** The frequency of splenic MDSCs in anti-PC or IgG mice at various stages of EAE progression was assessed by flow cytometry. Data are presented as means ± SEM (n > 3, * p < 0.05, ** p < 0.001 by Student *t* test). The absolute cell counts of (**G)** splenic MDSCs and the two (**H)** MDSC subsets from both groups are presented as means ± SEM (n > 3, ** p < 0.01). (**I)** The expression of cell surface markers on splenic MDSCs were assessed by flow cytometry. Expression levels are presented as histograms (upper panel) and as means ± SEM (lower panel, n > 3, * p < 0.05).

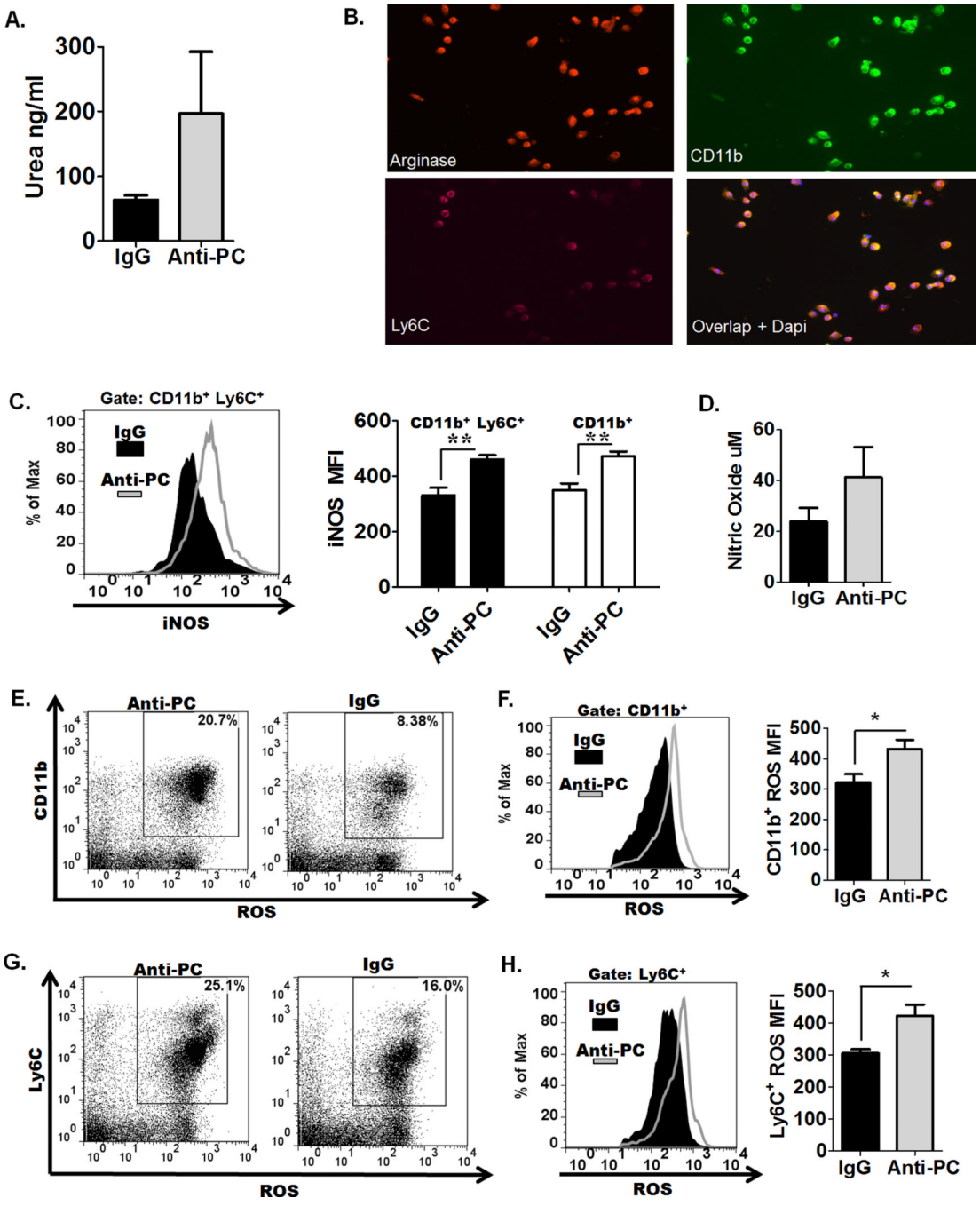

Figure 5. CD11b$^+$ cells from anti-PC mice express high levels of factors that are known to T-cell-suppressive

(A) Splenocytes were collected following EAE induction, and arginase activity in splenocytes was measured based on urea generation. Data are represented as means ± SEM (n = 4). **(B)** Splenocytes were cultured on cover slips overnight, and cells were stained with fluorochrome-conjugated antibodies to CD11b, Ly6C, and arginase. Coverslips were mounted on slides, and images were captured using a Zeiss Axio Imager M1 microscope. **(C)** The expression of iNOS in CD11b$^+$ and CD11b$^+$ Ly6C$^+$ cells was assessed by flow cytometry. Left panel show the flow cytometric histogram of iNOS expression in CD11b$^+$ Ly6C$^+$ cells. Right panel represents the mean fluorescence intensity (MFI) of iNOS

expression in $CD11b^+Ly6C^+$ and $CD11b^+$ cells. Data are represented as means ± SEM (n = 3; ** $p < 0.01$ by Student *t* test). **(D)** Splenocytes were cultured for 48 hours, and supernatants were collected to assess NO production by Griess assay. Data are represented as means ± SEM (n = 3). **(E– H)** ROS generation was assessed by incubating splenocytes with 2',7' –dichlorofluorescein diacetate. Degree of cell fluorescence, which increases with elevated ROS generation, was assessed by flow cytomerty. The frequencies of ROS-positive **(E)** $CD11b^+$ cells and **(G)** $Ly6C^+$ are shown as flow cytometric dot plots. The levels of ROS generation in $CD11b^+$ cells **(F left panel)** cells and $Ly6C^+$ cells **(H left panel)** are shown as histograms, and the MFI correlating to ROS generation in $CD11b^+$ cells **(F right panel)** and $Ly6C^+$ cells **(H right panel)** are represented as means ± SEM (n = 4; * $p < 0.05$).

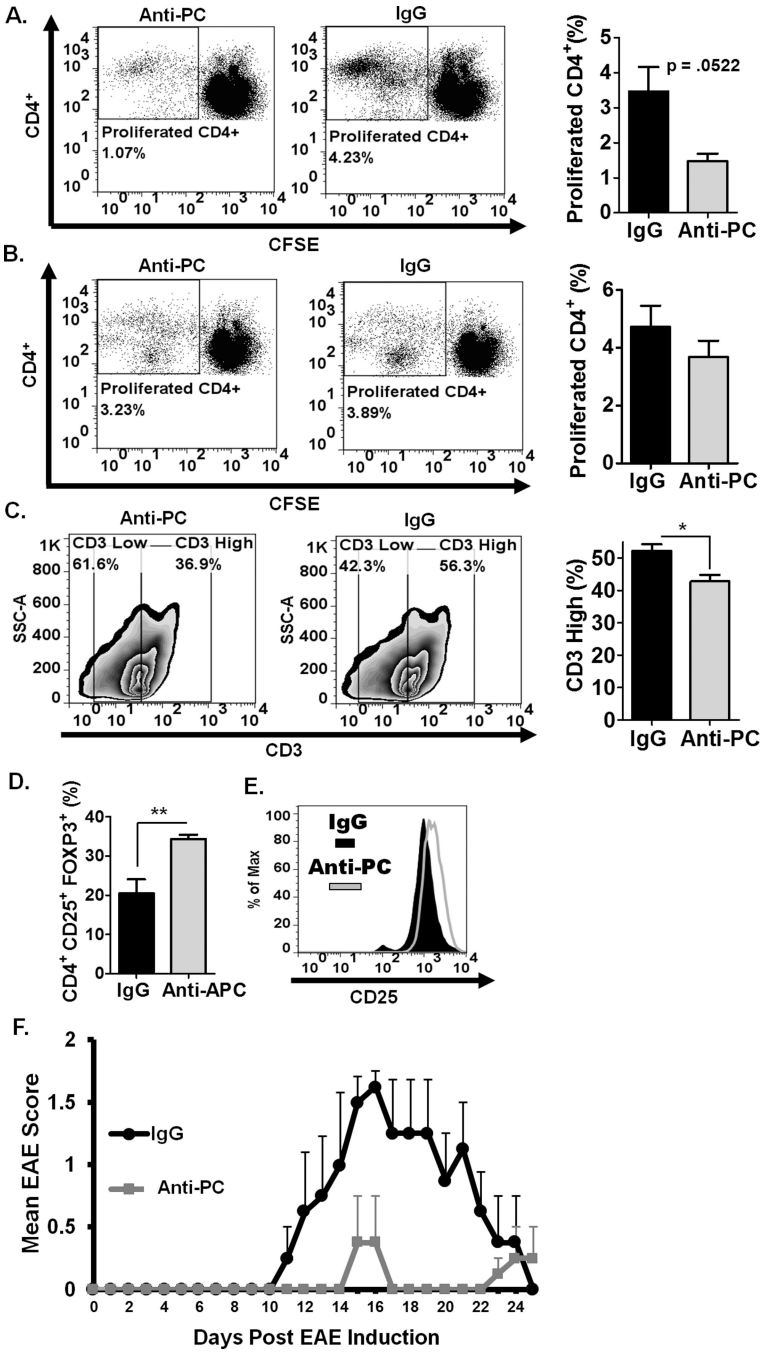

Figure 6. CD11b$^+$ cells from anti-PC mice suppress CD4$^+$ T-cell proliferation and increase CD4$^+$ T-regulatory cells

(A) Following EAE induction, splenic CD11b$^+$ isolated from anti-PC or IgG mice were co-cultured for 96 hours with $MOG_{35–55}$-specific CD4$^+$ T-cells isolated from BL/6 2D2 mice. To assess proliferation, CD4$^+$ T-cells were labeled with CFSE and stimulated with $MOG_{35–55}$. CFSE dilution was assessed by flow cytometry. Left panel represents flow cytometric dot plot of CFSE labeled CD4$^+$ T-cells co-cultured with CD11b$^+$ cells from either anti-PC or controls. Right panel shows percentage of CD4$^+$ T-cells that have proliferated based on CFSE dilution. Data are represented as means ± SEM (n = 3; p calculated by Student *t* test). **(B)** Non-CD11b$^+$ splenocytes from anti-PC or control mice

were co-cultured for 96 hours with $CD4^+$ T-cells from BL/6 2D2 mice. $CD4^+$ T-cells were labeled with CFSE and stimulated with $MOG_{35–55}$ for 96 hrs. Proliferation of $CD4^+$ T-cells was analyzed by flow cytometry based on CFSE dilution. Left panel represents flow cytometric dot plot of CFSE labeled $CD4^+$ T-cells co-cultured with non-$CD11b^+$ cells from anti-PC or control mice. Right panel shows percentage of $CD4^+$ T-cells that have proliferated based on CFSE dilution. Data are represented as means ± SEM (n = 3). (**C**) The expression of cell-surface CD3 on $CD4^+$ T-cells that were co-cultured with $CD11b^+$ cells from either anti-PC or control mice was assessed by flow cytometry. Left panel shows the expression levels of CD3 as flow cytometric contour plots (gated on CD3 cells), and the MFI corresponding to CD3 levels are shown as mean ± SEM on right panel (n=4; * $p < 0.05$ by Student *t* test). (**D-E**) $CD11b^+$ cells were isolated from anti-PC or IgG mice following EAE induction, and co-cultured for 96 hours with $CD4^+$ T-cells that were stimulated with plate-bound anti-CD3 and soluble anti-CD28. **(D)** After co-culture, the frequency of T-regs among $CD4^+$ T-cells was assessed by flow cytometry, and data are represented as means ± SEM (n = 3; * $p < 0.05$ by Student *t* test). **(E)** The expression levels of CD25 on T-regs were assessed by flow cytometry. Data are presented as flow cytometric histogram. **(F)** $CD11b^+$ cells isolated from IgG or anti-PC were adoptively transferred to EAE recipient mice on days 3 and 7 post EAE induction. The progression of EAE was monitored daily by assessing clinical signs. Scores were plotted as means ± S.E.M (n = 4).

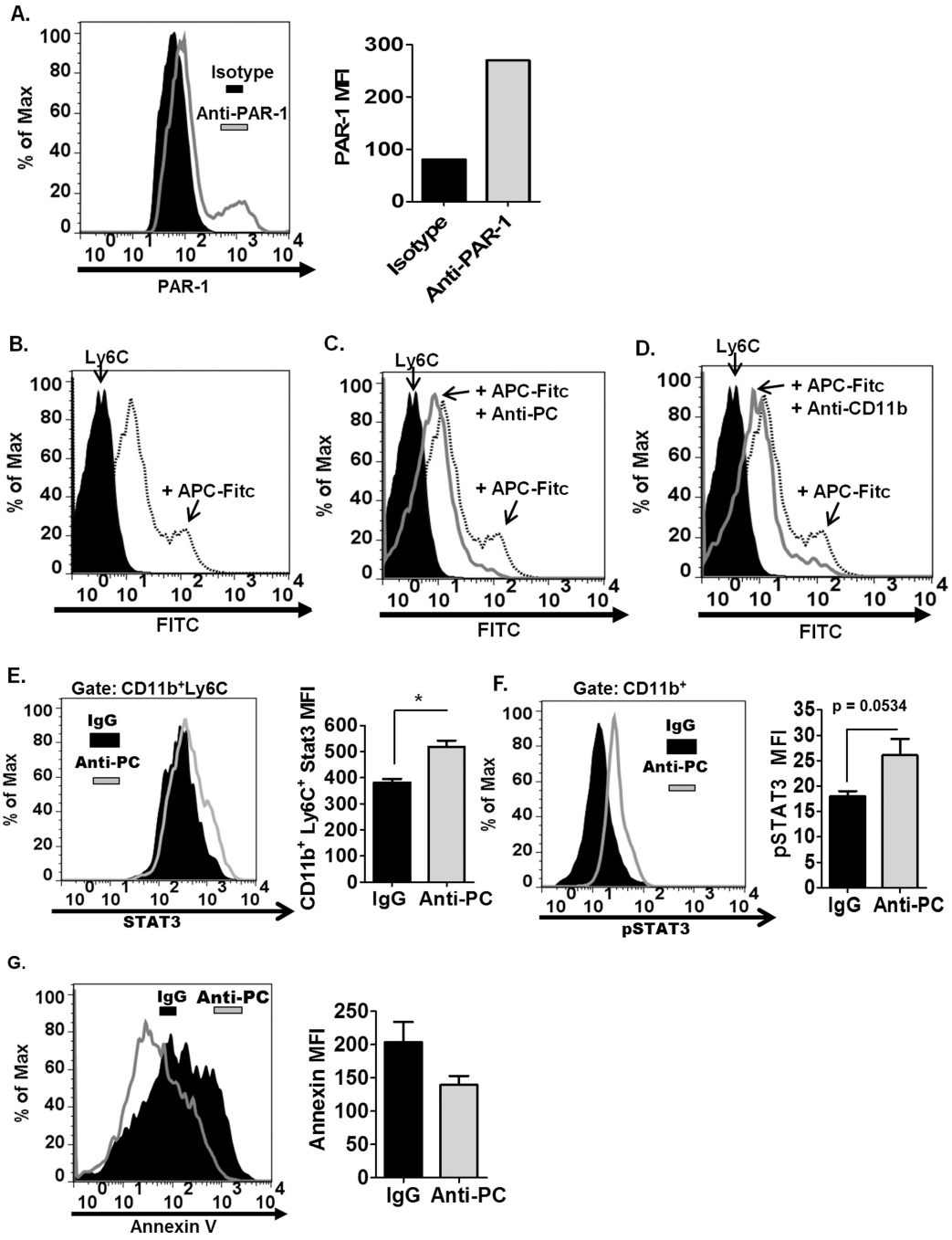

Figure 7. APC directly binds Ly6C$^+$ cells

(A) The expression of PAR-1 on the surface of Ly6C$^+$ cells is assessed by flow cytometry. Left panel shows the histogram representation of PAR-1 expression on Ly6C$^+$ cells. Right panel shows the graphical representation of MFI corresponding to PAR-1 expression on Ly6C$^+$ cells. (**B**) To determine whether APC can directly interact with Ly6C$^+$ cells, fluorochrome-conjugated APC were incubated with splenic cells, and the binding of APC to Ly6C$^+$ cells was assessed by flow cytometry (gated on Ly6C$^+$ cells). (**C**) To examine whether anti-PC can decrease the interaction of APC to Ly6C$^+$ cells, fluorochrome-conjugated APC were incubated with splenic cells with or without anti-PC, and the binding

of APC to $Ly6C^+$ cells was assessed by flow cytometry. (**D**) To examine whether APC utilizes the CD11b integrin to bind to $Ly6C^+$ cells, fluorochrome-conjugated APC were incubated with splenic cells with or without anti-CD11b, and the binding of APC to $Ly6C^+$ cells was assessed by flow cytometry. **(E)** Stat3 expression in splenic $CD11b^+Ly6C^+$ cells was assessed by flow cytometry. Left panel shows the histogram representation of Stat3 expression in $CD11b^+Ly6C^+$ cells from anti-PC and control mice. Right panel is the graphical representation of the MFI corresponding to Stat3 expression in $CD11b^+Ly6C^+$ cells. Data are represented as means ± SEM ($n = 4$; * $p < 0.05$ by Student t-test). **(F)** The phosphorylation status of Stat3 in $Ly6C^+$ cells was assessed by flow cytometry. Levels of phosphorylated Stat3 (pStat3) in $Ly6C^+$ cells from anti-PC and control mice are represented as flow cytometric histograms (left panel) and as mean MFI ± SEM (right panel, n=3; p calculated by Student t-test). **(G)** Apoptotic $CD11b^+Ly6C^+$ cells from both anti-PC or IgG mice was assessed by annexin V binding. The degree of annexin V binding to $CD11b^+Ly6C^+$ cells was examined by flow cytometry, and levels of annexin V binding are shown as flow cytometric histograms (left panel) and as mean MFI ± SEM (right panel, n =4).